CHAPTER

Wildfires, haze, and climate change

10

Maggie Chel Gee Ooi[1], Andy Chan[2], Mohd Talib Latif[3], Neng-huei Lin[4,5] and Li Li[6]

[1]Institute of Climate Change, Universiti Kebangsaan Malaysia (UKM), Bangi, Selangor, Malaysia; [2]Department of Civil Engineering, University of Nottingham Malaysia, Semenyih, Selangor, Malaysia; [3]Department of Earth Sciences and Environment, Faculty of Science and Technology, Universiti Kebangsaan Malaysia (UKM), Bangi, Selangor, Malaysia; [4]Department of Atmospheric Sciences, National Central University, Zhongli District, Taoyuan, Taiwan; [5]Center for Environmental Monitoring Technology, National Central University, Zhongli District, Taoyuan, Taiwan; [6]School of Environmental and Chemical Engineering, Shanghai University, Baoshan, Shanghai, China

Chapter outline

Handbook of Energy and Environmental Security. https://doi.org/10.1016/B978-0-12-824084-7.00013-8

1. Introduction

The future climate is expected to become hotter, with an anticipated rise of global temperature by 1.5 to 2°C comparing with preindustrial level (IPCC, 2014). This range naturally depends on the anthropogenic emission scenario: whether it is the representative concentration pathway (RCP) or the more recently introduced shared social pathway. The weather extremes will intensify and threaten the well-being of the people and exacerbate wildfire burning. The occurrence of wildfire has gradually become an annual occasion where the severity of extreme wildfires seems to have continuously escalated. The period of burning has also increased, and the fire season has been found to occur earlier than usual (Wuebbles et al., 2017). The climate change conditions with increased temperature, drought, and weather anomalies might create long-term change to the burning condition with higher fire risk.

In 2020 alone, the Southeast Asian fire, Amazon rainforest wildfires, Australia bushfires, and the California gigafire have clearly shown that the scales of destruction have tremendously intensified. The environmental and economic implications of biomass burning incidents are naturally detrimental. Wildfires damage the biodiversity-rich wilderness, threaten the habitat and livelihood of animals and plants, although it is still hard to quantify the actual statistics of the impact of wildfires on biodiversity to date (Michelle et al., 2020). The impact does not stop at the pristine forest loss, but also upsets the balance of the ecosystem, the carbon cycle, the hydrological cycle, and natural habitat to flora and fauna and their consequences (See Table 10.1). The postburning residues also increase the sedimentation of the river and stream, leading to flooding which would further degrade the soil fertility (Daniel et al., 2008). The economic damage is enormous from the disaster response stage which involve evacuation and relief effort, relocation, personnel mobilization, to postmortem recovery on destruction of properties and infrastructure, insurance claim, and the less tangible health and environmental cost. Table 10.1 tabulates information of wildfire coverage and implications.

When biomass burning haze (BBH) occurs, the mixture of burning gases and aerosol suspends in the atmosphere and reduces overall visibility. It is the largest source of primary fine carbonaceous aerosols and second largest source of trace gases (Akagi et al., 2011). The fire emissions released are mainly made up of burning aerosols, trace gases (CO_2, CO, NO_x, O_3, etc.) and toxins (persistent organic pollutants) that especially threaten human health (Chen et al., 2017). This becomes even more daunting when the burning occurs in the forest and on peatland, which are one of the largest natural terrestrial carbon reserves (Turetsky et al., 2015). The burning releases greenhouse gases (CO_2, O_3, and H_2O), which continue to warm up the ambient temperature and form a positive radiative forcing feedback loop to warm the atmosphere. On the other hand, the biomass burning also produces large amount of aerosol below the size of 2.5 μm ($PM_{2.5}$) and has the tendency to alter the radiative forcing, cloud properties, and precipitation formation (Andreae et al., 2004). Depending on circumstances in which immense amount of haze is produced, the changes on radiative balance and hydrometeorological processes would create regional climate-forcing effects.

The relationship of wildfires haze on weather and climate is discussed in Section 2. Section 3 guides through the basics of burning to understand the burning sources (burning types, fuel types, fire types, and fire spread) with relevant fire haze characteristics produced and weather that are conducive for the fire occurrence and propagation. Case study is provided in Section 4 to explain the uniqueness of wildfire burning regions and their corresponding haze formation. Mitigation and preventive

Table 10.1 Summary of the social, economic, and environmental implications of the recent wildfires.

Wildfire event	2015 Southeast Asian haze	2018 California wildfire	2019 Amazon rainforest wildfire	2019–20 Australia bushfires	2019–20 Arctic fire
Areas affected	Indonesia, Singapore, Malaysia	California	Amazon	Australia	Eastern Russia and Alaska
Land area destroyed	More than 2.6 million hectares	Up to 0.8 million hectares (Porter et al., 2020)	Up to 0.9 million hectares burnt (CBS News, 2019)	More than 12.6 million hectares burnt (Werner and Lyons, 2020)	More than 14.8 million hectares burnt (McCarty et al., 2020)
Loss of human lives	At least 19 fatalities (McKirdy, 2015)	At least 103 fatalities (Porter et al., 2020)	–	At least 33 fatalities (BBC News, 2020)	–
Loss of properties	–	22,868 structures destroyed (Porter et al., 2020)	Homes of indigenous tribe	More than 2000 houses destroyed (Werner and Lyons, 2020)	–
Other environmental implication	Loss of forest, peat, and other land; costs related to biodiversity may exceed US $295 million for 2015 (World Bank Group, 2015)	–	Millions of animals and biodiversity	11.3 million Australians affected by smoke (Werner and Lyons, 2020); over one billion animals were killed (Werner and Lyons, 2020)	Melting of ice sheet, permafrost, etc. (McCarty et al., 2020)
Economic cost	Up to $16.6 billion USD (World Bank Group, 2015)	More than $150 billion USD (Wang et al., 2020)	More than $957 billion USD (Gill, 2020)	$75 billion USD (Quiggin, 2020)	–
CO_2 emitted	Up to 1150 million tonnes (Harris et al., 2015)	68 million tonnes (U.S. Department of the Interior, 2018)	154 million tonnes (Zuckoff, 2019)	434 million tonnes (Werner and Lyons, 2020)	Up to 244 megatonnes (Witze, 2020)

measures need to be taken to prevent and alleviate the potential wildfire risk and their haze implications. Section 5 provides an overview of available fire prediction models and is also discussed for their application and status. Section 6 discusses the future projection of the fire condition due to the changing climate condition and the potential implication and outlook.

2. Relationship between wildfires haze and climate

The Earth's climate is subjected to change by external physical factors known as climate forcing. These factors such as the changes in solar and anthropogenic activities do not preexist in the climate system, and hence their presence would induce changes to the existing system. One of the greatest factors which causes the climate change to take place is the change in radiative forcing, i.e., the energy budget distribution within the earth-atmosphere system. Apart from the direct radiative forcing, the burning aerosols emitted from biomass burning also exhibited a more complex role as an indirect effect of cloud interactions.

2.1 Direct radiative forcing

The emission from biomass burning contributes to both positive and negative radiative forcing. Among the components that contribute to the relative radiative forcing shown in Fig. 10.1, emission from

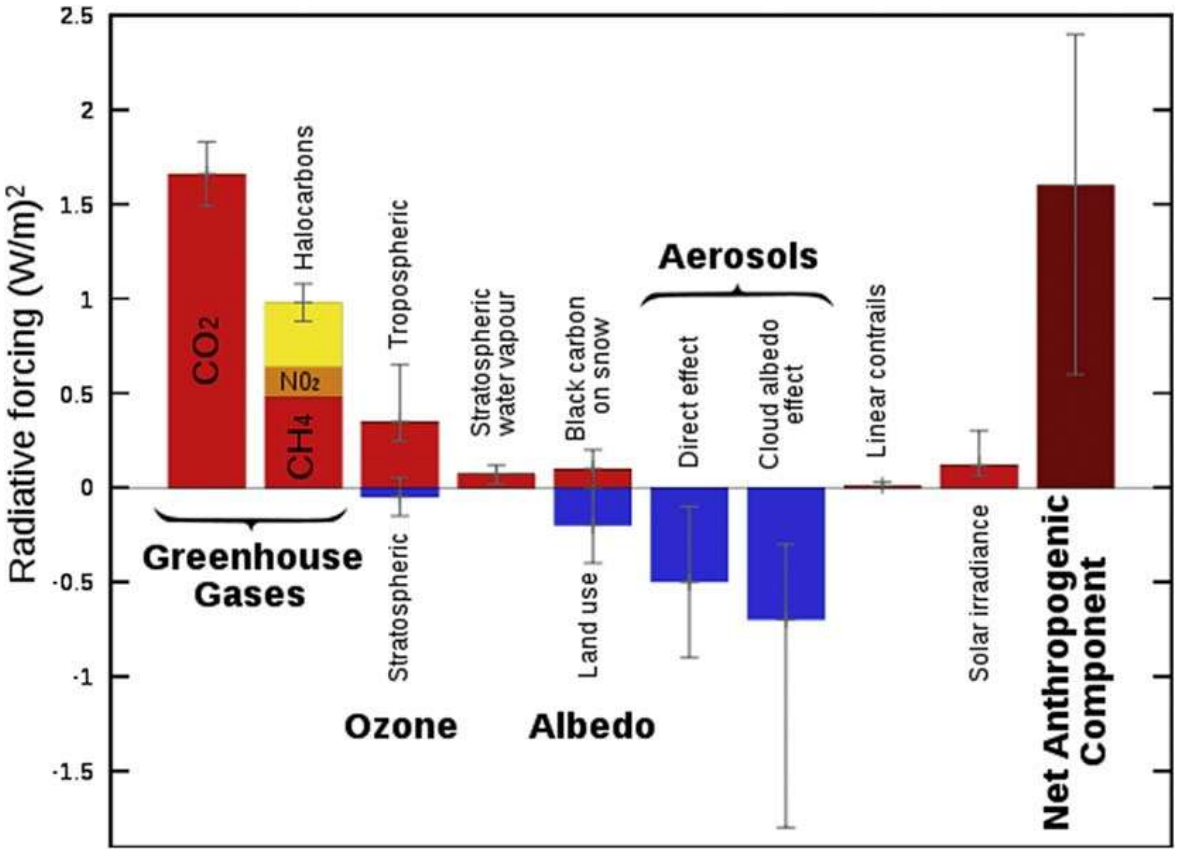

FIGURE 10.1

The relative radiative forcing of the Earth system contributed by different components.

Source: Leland McInnes (https://commons.wikimedia.org/wiki/File:Radiative-forcings.svg), "Radiative-forcings," https://creativecommons.org/licenses/by-sa/3.0/legalcode.

combustion has contributed to the positive forcing by greenhouse gases emission (CO_2), tropospheric ozone (O_3), black carbon (BC) deposited on snow as well as negative forcing by cleared land use and burning aerosols. CO_2 is known to be the main greenhouse gas that absorbs and retains heat from the sunlight and increases the atmospheric temperature. In this context, CO_2 is a product of complete combustion of the biomass. Considering the amount of CO_2 captured by plants during the photosynthesis process, the amount of CO_2 released back to the atmosphere is able to offset its carbon footprint, as well as its radiative forcing.

Biomass burning aerosol (BBA) pollutant has a more multifacet radiative forcing properties depending on the particle sizes distribution, optical properties, hygroscopicity, etc (Chen et al., 2017). Particulate matters ($PM_{2.5}$ and PM_{10}) make up the main compositions of the burning aerosol emission. The chemical constituents of the aerosols are complex, including the carbonaceous aerosol, ions, and organic compounds. The direct aerosol radiative forcing is mainly determined through the amount of aerosol loading and optical properties of aerosol including the single scattering albedo (reflectivity), specific extinction coefficient (absorption), and the scattering phase function (shape). The shadowing effect from thick biomass burning plumes with high aerosol optical depth (AOD) is able to scatter and attenuate light, and hence create a regional cooling effect on the surface beneath. The global BBA is found to contribute to -0.3 Wm^{-2} direct radiative cooling compared to the $+2.45$ Wm^{-2} from the anthropogenic greenhouse gases (Hobbs et al., 1997).

In general, the direct effect of BBA attenuates and negatively forces the solar radiation, while the carbonaceous component in the aerosol emitted contributes otherwise. Among which, the BC and brown carbon (BrC) absorb solar radiation as positive radiative forcing component (Ramanathan and Carmichael, 2008). Due to the short atmospheric lifetime of BBA, the effect of radiative heating might be short-term. When dark-coloured BC is deposited over surface of high albedo, such as snow and ice cover, it is able to absorb heat and accelerate the heating and melting of these surfaces (Kang et al., 2020). Nevertheless, anthropogenic emission also produce large amount of BC which cause the uncertainties on the exact amount of BC contributed by biomass burning. Similarly, the BrC, a yellowish/brownish light-absorbing organic carbon is also known for its heat-absorbing capability in the fresh BBH up to 30% of the total radiation absorption (Wang et al., 2018; Pani et al., 2021) (Fig. 10.2).

2.2 Indirect effect

Aerosol also serves as a cloud condensation nuclei (CCN) on the microphysical processes of cloud formation and its interaction with clouds, which are known as indirect effects. The incomplete combustion of biomass burning releases different organic compounds, the largest component of BBAs. The degradation of cellulose, lignin, and conifer through burning produces organics such as levoglucosan, methoxyphenols, and dehydroabietic acid, respectively (Simoneit, 2002). Majority of these organic aerosols are hygroscopic due to the presence of polar functional groups, which make them an efficient cloud droplet nucleate, and participant in the indirect effect. The presence of water-soluble ions such as sulfate, nitrate, and ammonium are also able to alter the hygroscopic properties of the aerosol particles. The aerosol particle size in accumulation mode (0.1 to 1 μm dry diameter) is known to be efficient CCN under humid conditions.

There is the first indirect effect, also known as cloud albedo effect in which aerosol affects the cloud optical properties and the second indirect effect, also known as the cloud lifetime effect in which aerosol is involved in the precipitation efficiency of the cloud. In the first indirect effect, the aerosol

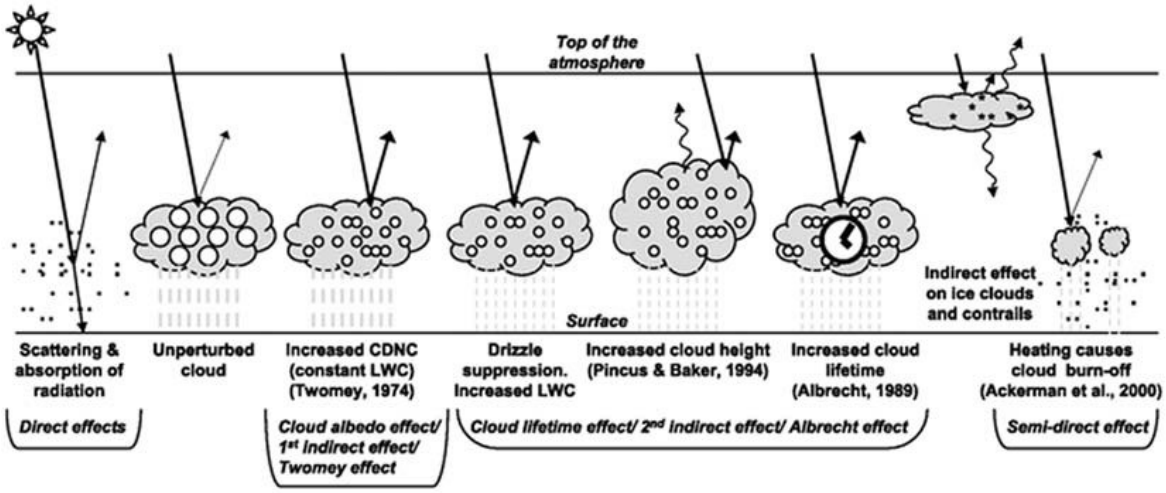

FIGURE 10.2

The aerosol radiative and climate forcing effect.

Source: IPCC Fourth Assessment Report: Climate Change 2007, Working Group I: The Physical Science Basis, Chapter 2: Aerosol, Figure 2.10.

acts as CCN with no change to the amount of liquid water content. Under such circumstances, the cloud droplet formed with BBA are much smaller than the natural aerosols exist. The larger amount of BBA as CCN increases the amount of cloud droplet form and hence increases the albedo of the cloud, from which the amount of radiation reduces reaching the atmosphere beneath.

In the second indirect effect, the precipitation efficiency and lifetime of the cloud are changed due to the change of the droplet number concentration. However, high concentration of BBA and smaller cloud droplets inhibit warm rain processes, i.e., reduce rainout at the lower level clouds and even ice cloud. The water droplet is unable to grow due to the abundance of available CCN. With the continuous accumulation of the small cloud water droplet, the cloud continues to grow into higher altitude and takes a much longer time to rain out. The inhibition invigorates the updraft of polluted air mass, where the large size and solid or mixed state hydrometeors are formed with greater release of latent heat to continue the updraft process. The rainout from the upper level then causes severe thunderstorms (Rosenfeld et al., 2008).

The influence of second indirect effect on radiative forcing is much smaller compared to the precipitation effect. Nevertheless, due to the large uncertainties in the distinctive properties of each aerosol components in the atmosphere, the understanding regarding the precipitation is still limited.

3. Wildfire burning and haze formation conditions

In this section, we would like to dissect the wildfire from the burning emission to their connection with weather conditions. The amount of BBH emission is dependent on the size of burnt area, fuel characteristics, fire types, and weather conditions. The collective of these factors greatly affects the emission species especially the organic compounds produced during the degradation of fuel.

3.1 Fuel types

Biomass fuel is high in organic content and is prone to sustain burnings, while the mass determines how much will be burnt. It involves different layers of biomass including the tree canopy (hereafter includes emergent layer, canopy, and understory), undergrowth, surface, and below surface biomass. Above surface level, there are live fuels such as trees, shrubs, and grass that consist of wooden and seasonal herbaceous components. While on the subsurface, there is a layer of dead fuel, mainly consisting of dry leaf mass that is easier to burn due to the availability of ignition source. Under intensive deforestation, drainage, and drought, the water table level in the soil drops and causes the deep soil burning more prone to occur (Turetsky et al., 2015).

The geographical location is hence a good guide for the vegetation cover types (fuel types), amount burnt, and burning cycles. The burning fuel is usually categorized according to the land cover and biome types, for example, savanna/grasslands, shrublands, tropical forest, temperate forest, agriculture waste, boreal forest, and peat, depending on the classification used. Although similarly falling under tropics, the burning over Africa is very different compared to the Maritime Continent (MC) and Amazonia fire due to the burning activities and types of land cover involved. The savannahs over Africa plain are burnt naturally during the dry season to replenish the soil nutrients, and the region is acclimated to recover from such drought and burning cycles every year, with most burning in the Northern Africa in December to January and the Southern Africa in July to August. On the other hand, the burning over MC and Amazon are mostly human-induced burning activities and propel into uncontrollable fire during the dry season. The former occurs during the slash-and-burnt land clearing, where the burning of agricultural waste spreads to the burning of the underlying peatland between August and October. The latter occurs in August to September as a result of intense deforestation and agricultural waste burning which subsequently spread more uncontrollably into the more pristine rainforest (Giglio et al., 2013).

The amount of air pollutants emitted from the vegetation cover can be determined from the emission factor and the relevant activity factors. Emission factor is a dimensionless value on the amount of air pollutant that will be produced based on the activity factors such as dry biomass burnt, heat produced, period of burning, and area burnt. It is usually determined from field experiment and empirical methods. There are several emission factor databases available (Akagi et al., 2011; Andreae and Merlet, 2001) for application of the atmospheric community and fire emission inventories. The emission factor might be slightly different among the fire emission inventory due to the land use classification, but its deviation is not the main factor causing the difference between the fire inventories but the algorithm each inventory adopted (Liu et al., 2020).

The emission factors for several main trace gases and carbonaceous aerosols from GFEDv4s are shown in Fig. 10.3. The air pollutants are arranged from left to right according to the emission factor from the highest to the lowest. CO_2 is a product of complete combustion; hence, the emission factor does not vary much among different vegetation covers. Notably, the peatland has a relatively high emission factor for CO and CH_4 due to the high amount of carbon content and its incomplete burning condition. While the tropical peatland contains a higher carbon content (56%) compared to the temperature and boreal peat (44.2%), the burning of tropical peatland produces larger amount of trace gases (CO_2, CO, and CH_4) but slightly smaller amount of particulate matters (Hu et al., 2018). The uncertainties of the burning dynamics are attributed as the deviation of the emission factors.

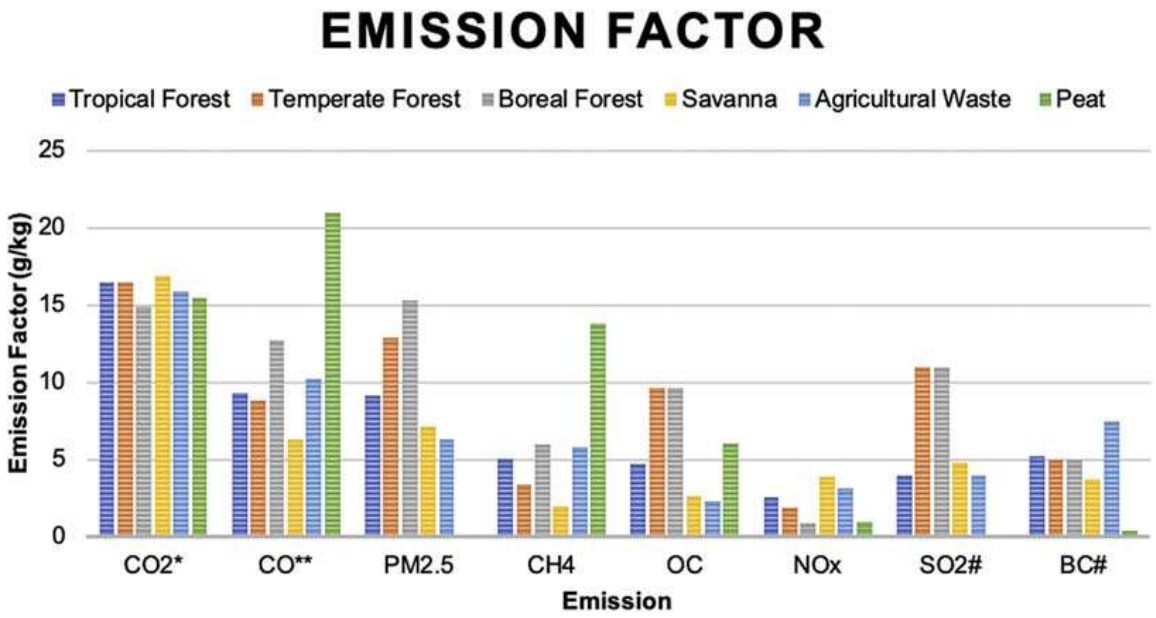

FIGURE 10.3

The emission factor of selected trace gases and aerosols extracted from GFEDv4.1s (Van Der Werf et al., 2017); symbols beside the pollutant name refer to scaled according to $^{*} = 10^{2}$, $^{**} = 10^{1}$, and $^{\#} = 10^{-1}$.

3.2 Fire types

There are two major types of fire involved in wildfire burning, the flaming and smoldering fire as shown in Fig. 10.4. The flaming fire when the burning occurs on and above the surface when combustion is complete. Due to the abundant oxygen supply, this fire occurs when the combustion is complete with high temperature and produces a large amount of heat. The heat difference between the burning plume and surrounding air and the atmospheric stability would determine the plumes rise. While the below-surface burning mainly consists of smoldering burning that occurs on the deeper soil layer. The smoldering fire can occur without any flames and also at much lower peak temperature of 450–700°C compared to flaming (1500–1800°C) with three times smaller heat fluxes required as ignition source (Santoso et al., 2019). While both fire types are distinct, they can lead to one another. Residual fire is the transition of flaming fire into smoldering fire where the remaining of the residue or below-ground biomass is burnt and the amount of heat generated is much lesser than direct flaming. On the other hand, the smoldering fire has the tendency to transform into flaming fire under unfavourable dry and strong wind conditions.

In areas like the Arctic and the MC, the peatland with high organic content can sustain for a tremendously long period due to the low temperature, causing these flameless burning conditions that are difficult to detect (Huang and Rein, 2019). Over the Arctic region, the burning happened during the boreal summer, but the burning emission has started earlier in the year 2019 and 2020 due to the early thawing and warming of temperature. Interestingly, the burning does not start on the surface but resurfaces from peatland and permafrost burning that has sustained underground over months and years (McCarty et al., 2020). It would be easier to detect the flaming and residue fire from the satellite observation due to the higher heat, while it is difficult to detect the smoldering fire directly from satellite observation. The aerosol retrieval method is generally used to identify the smoldering fire.

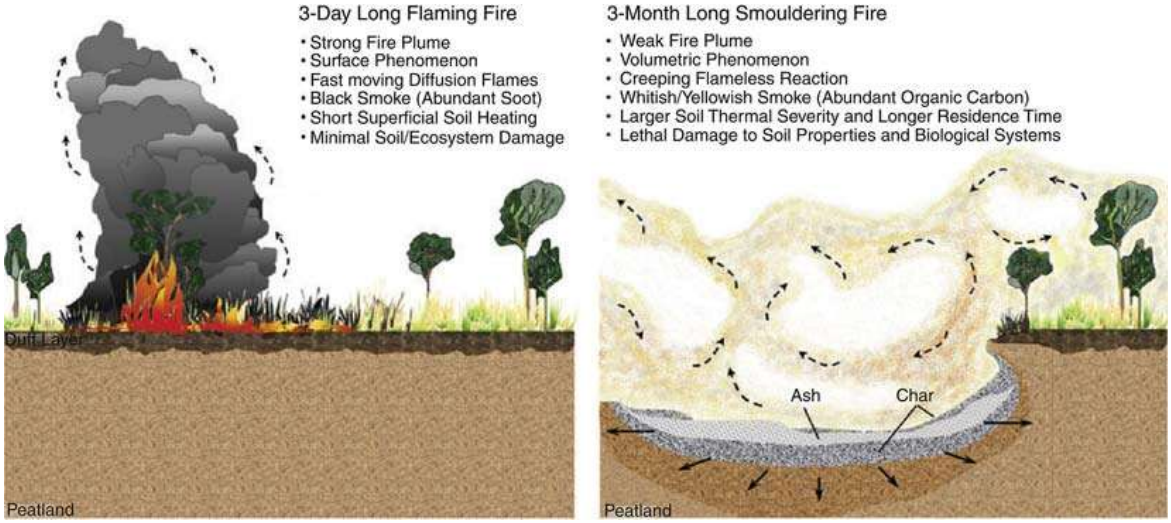

FIGURE 10.4

The emissions formed from flaming and smoldering fire.

Directly extracted from (Hu et al., 2018).

3.3 Fire spread

The burning fuel can change along the progress of the fire spread. The near surface and canopy wind determine the direction of the fire spread. The heat generated from the fire is able to heat and prepare the fuel to burn easily when the fire arrives. Under strong wind conditions, the burning residue or ember is able to be lifted and spread to a new burning spot, which is known as spotting. While the crowning is a process of fire spreading along the tree canopies, the fire spreading rate might be accelerated when there is incidence of strong wind gust or updraft, for example, near the mountain due to the availability of mountain-valley winds. Under circumstances where the spread has directed toward the forest region would cause great destruction to the pristine natural resources as occurred during the burning in MC peatland burning and Amazon forest fire. Conversely, when the fire spreads toward the populated residential or commercial regions, it can cause large economic properties and life loss.

The role of meteorological condition has previously contributed to a large-scale fire spread of burning seasons over Southern California. The strong and dry Santa Ana winds have contributed to the burning season in October to April. The dry katabatic winds that originate from the inland Great Basin have blown toward the coastal Southern California, a highly populated urban area (Jin et al., 2015). The wind intensified the fire burning condition and accelerated the spreading of fire by three times toward the populated coastal area. On a smaller scale, the strong storm updraft of the dry wind has evolved the fire into fire tornado that had happened during Woolsey and Carr fire in 2018. It has totaled up an estimate of 150 billion USD appreciable economical losses during the 2018 California fire (Wang et al., 2020).

3.4 Weather anomaly

The drought condition is the predominant factor leading to burning. It comprises different types of droughts, namely weather drought, agricultural drought, and hydrological drought. The weather drought has indirect influence on the agricultural drought and hydrological drought. Under weather drought conditions, the agricultural drought might exacerbate affecting the agricultural cultivation and vegetation to wilt and from which increases the fuel availability. Similarly, the weather drought causes the reduction of soil water moisture and water table that lead to the continuity of burning to spread. Precipitation has occurred less frequently to alleviate and stop the propagation of the fire burning. Weather anomaly is a condition where the weather is different from the long-term average baseline climate variability. Positive temperature anomaly is often related to the aforementioned weather drought condition that influences the temperature and precipitation. Such a natural regulatory phenomenon that is commonly related to biomass burning are the weather anomalies on different time scale: intraseasonal scale (e.g., Madden–Julian Oscillation (MJO) (Amirudin et al., 2020), Southern Annular Mode (SAM) (Harris and Lucas, 2019)), interannual scale (e.g., El-Niño Southern Oscillation (ENSO), Indian-Ocean Dipole (IOD)), and interdecadal (Atlantic Multidecadal Oscillation (AMO) (Brando et al., 2019)). Among which, the influence of the interannual weather anomalies are known to be closely related to burning in different regions.

The El-Niño condition is the warm phase in which the eastern and central tropical Pacific Ocean (ecTPO) experienced a higher sea surface temperature (SST) compared with the western tropical Pacific Ocean (wTPO). During ENSO, the warm air above the ecTPO rises, while the cold air over the northern south America and wTPO sinks as seen in Fig. 10.5. The former, where the Amazon is located and the latter, where the equatorial Southeast Asia (SEA) and Australia are located, hence experience a warm and dry weather condition due to the sinking dry air. Such anomaly weather conditions are found to be related to the extreme wildfire over the SEA peatland fire, East Australia bushfire, and Amazonian forest fire, creating a conducive environment for burning. IOD is also a condition of SST anomaly but happens in the Indian Ocean (IO). During the positive IOD, the western (eastern) IO experiences an above- (below-) averaged SST which leads to a rising (sinking) air above the western (eastern) IO. The eastern IO where the MC and the Western Australia is located has hence experienced a drier, warmer, and fire-conducive atmospheric condition.

ENSO is an interannual event that occurred every two to seven years. It usually lasts for a year from its development in June-July-August until the March-April-May of the following year. While the positive IOD is also an interannual event that occurred on a shorter span and lasted for 5–6 months starting in June to November. When both of the ENSO and positive IOD coincided with the peak burning season in the MC region from September to October, it caused large amount of fire burning and hence producing large amount of emission (Amirudin et al., 2020). Similarly, it occurred for the Southwestern Australia when the weather condition becomes drier for the land to burnt and the fire to sustain and propagate (Harris and Lucas, 2019; Chang et al., 2021).

4. Wildfires haze conditions

The prevailing weather condition is important on the dispersion and transport of the emission produced from fire burning. The structure of the emission plume is important from which the amount of heat produced will be a large consideration of the emission structure. The emission structure determines the dispersion of the emission and the affected area on the downwind. Fig. 10.6 shows the amount of $PM_{2.5}$ emitted from fire burning depending on the geographical area based on the GFEDv4s dataset.

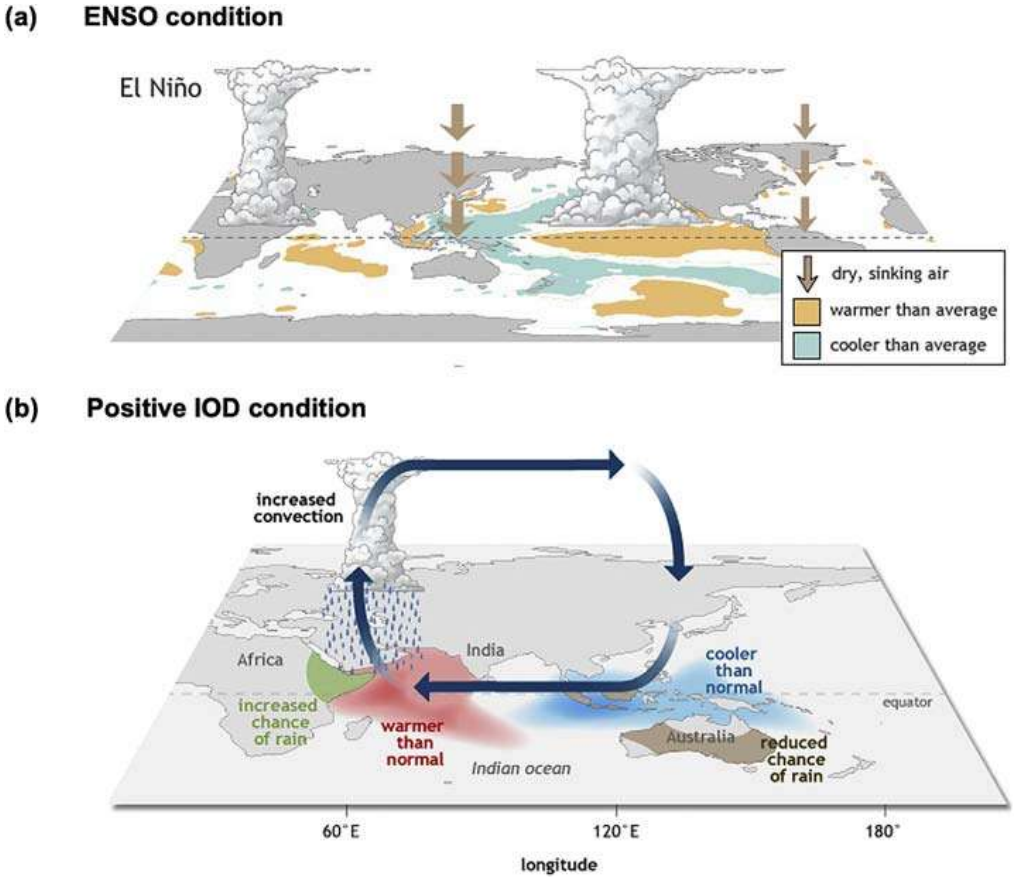

FIGURE 10.5

Illustration of atmospheric movement due to the (A) ENSO conditions (extracted from NOAA Climate.gov); (B) positive IOD condition.

Directly extracted from NOAA Climate.gov.

4.1 Fire emission inventories

There are two main approaches to develop the fire emission inventories: bottom-up and top-down approach. Bottom-up approach extracts fire emission information, either from satellite observations on land surface or local emission data, using the burned area method (e.g., FINN, GFED, and FLAMBE) or the fire radiative power (FRP) (e.g., GFAS and GBBEP-Geo). While top-down approach extracts fire emission information from the satellite observation based on the atmospheric structure, by using the FRP-based information and calibrate with satellite-derived dataset (e.g., QFED). The comparison of the selected four main fire emission inventories widely used is compiled in Table 10.2. These global fire emission inventories are mainly developed from the products extracted from Moderate Resolution Imaging Spectroradiometer (MODIS). Nevertheless, the amount of emission produced for different region can vary by several orders due to the interpretation and assumption of each emission inventories which can be easily compared through the FIRECAM google engine tool

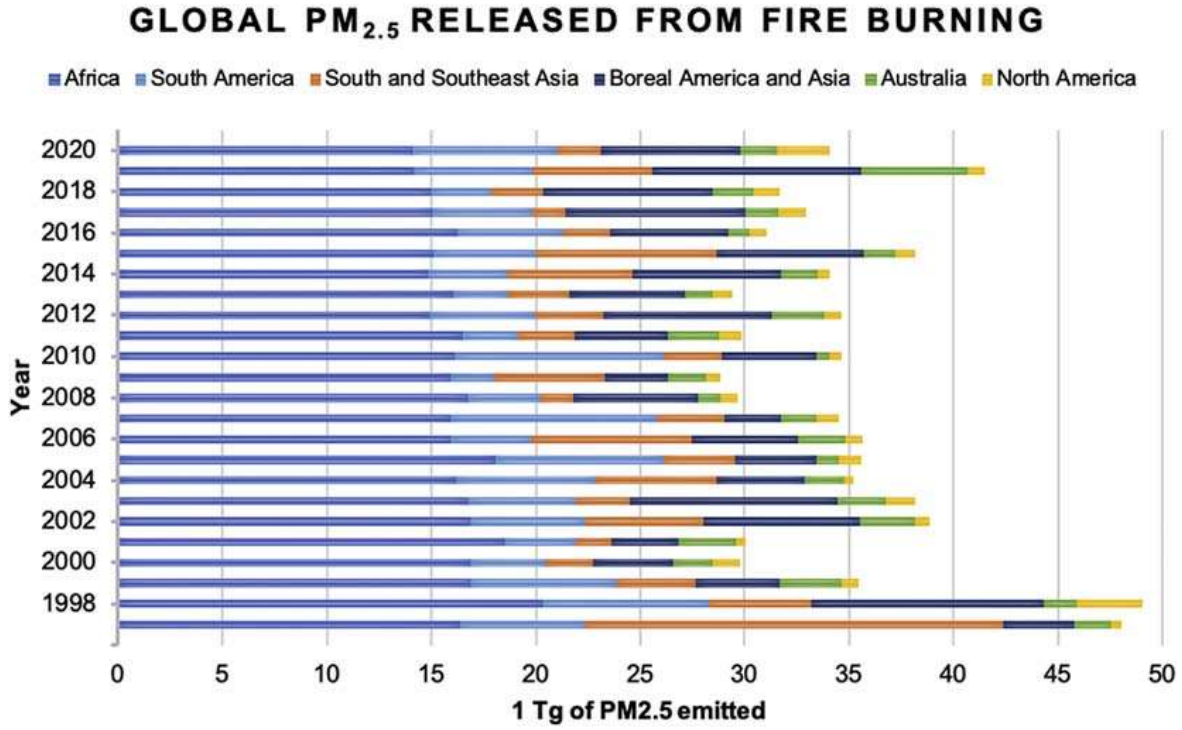

FIGURE 10.6

Global CO_2 emitted (in Tg) from fire burning according to Global Fire Emissions Database version 4.1 including small fire burned area (GFED4s).

(Liu et al., 2020). It has been attributed the difference between the emission inventories to few main factors including (i) the reliance on satellite fire products whether it is active fire or burnt area, (ii) missing satellite fire products due to cloud or haze cover, and (iii) difficulties in detection of small fires and others (Liu et al., 2020).

4.2 Case study: Peninsular Southeast Asia

The burning that occurs in the northern part of the SEA during the spring (December–April) annually has a much wider area of burnings across countries such as Myanmar, Thailand, Vietnam, and Laos. The burning is mainly initiated by human activities and the lack of soil moisture, while the dry weather condition spreads the burning further. The burning is escalated by the subsidence of dry air from higher latitude Tibetan Plateau. The strength of the dry air increases with the intensification of the India–Burma trough which is also connected to the ENSO of previous winter (Huang et al., 2016). The burning region over the western Myanmar and Thailand hence receives the inflow dry air to continue to fuel the burning.

The BBH from the spring burning over northern SEA can be lifted up to height of 700–800 hPa, approximately 2 km to 3 km due to the mountainous terrestrial condition and low-pressure trough present (Yen et al., 2013; Ooi et al., 2021). The strong lifting mechanism is able to carry the emission

Table 10.2 Comparison of fire emission inventories (GFEDv4s, QFED, FINNv1.5, and GFASv1).

	GFEDv4s	FINNv1.5	GFASv1.2	QFEDv2.5r1
Method	Bottom-up: burned area	Bottom-up: active fire	Top-down: FRP	Top-down: FRP with AOD data
Spatial Res	0.25° × 0.25°	1 km × 1 km	0.5° × 0.5°	0.1° × 0.1°/0.25° × 0.25°
Temporal resolution	Monthly (1995-NRT)	Daily (2002-NRT)	Daily (2001-NRT)	Daily (March 2000-NRT) (lag by six months)
Species	40 species of trace gases and aerosols	15 species plus NMOC that are speciated with MOZART (28), SAPRC99 (30), and GEOS-CHEM (11) chemical mechanism	42 species	17 species
Algorithm (see below for explanation)	BA × FL × CF × EF	BA × FL × CF × EF	FRE × beta × EF	FRP × beta × EF
Burned area estimate (BA); Fire radiative power (FRP) (MJ/km^2)	(BA) Active fire from MODIS fire observation; correction with MODIS burned area in some regions to include small fires	(BA) Active fires from MODIS Terra/Aqua; 1 km^2 for burned area and 0.75 km^2 for grassland/savanna	(FRP) FRP from MODIS Terra/Aqua	(FRP) FRP from the MODIS Level 2 fire products (MOD14 and MYD14) and the MODIS Geolocation products (MOD03 and MYD03)—according to biome types (4 LCs); cloud correction method by GFASv1 but more advanced treatment
Fuel loading (FL) [g/m^3]	CASA biogeochemical model (same with GFEDv3)	Land Cover map (MODIS LCT and VCF)—5 LCs (Hoelzemann et al., 2004)	–	
Combustion factor (CF) [-]/conversion factor (beta) [-]	(CF) Moisture condition for each fuel type (same with GFEDv3)	(CF) Function of tree cover (Ito and Penner, 2004; Wiedinmyer et al., 2006)	(beta) Link FRP in GFASv1.0 with dry matter combustion rate in GFEDv3/v4	(beta) Compared to GFED product
Emission factor (EF) (-)	(Akagi et al., 2011; Andreae and Merlet, 2001)	(Akagi et al., 2011; Andreae and Merlet, 2001) and others (Wiedinmyer et al., 2011)	(Andreae and Merlet, 2001) with updates (Kaiser et al., 2012)	GFEDv2 but calibrated with MODIS AOD data
Reference	Van Der Werf et al. (2017)	Wiedinmyer et al. (2011)	Kaiser et al. (2012)	Darmenov and da Silva (2015)

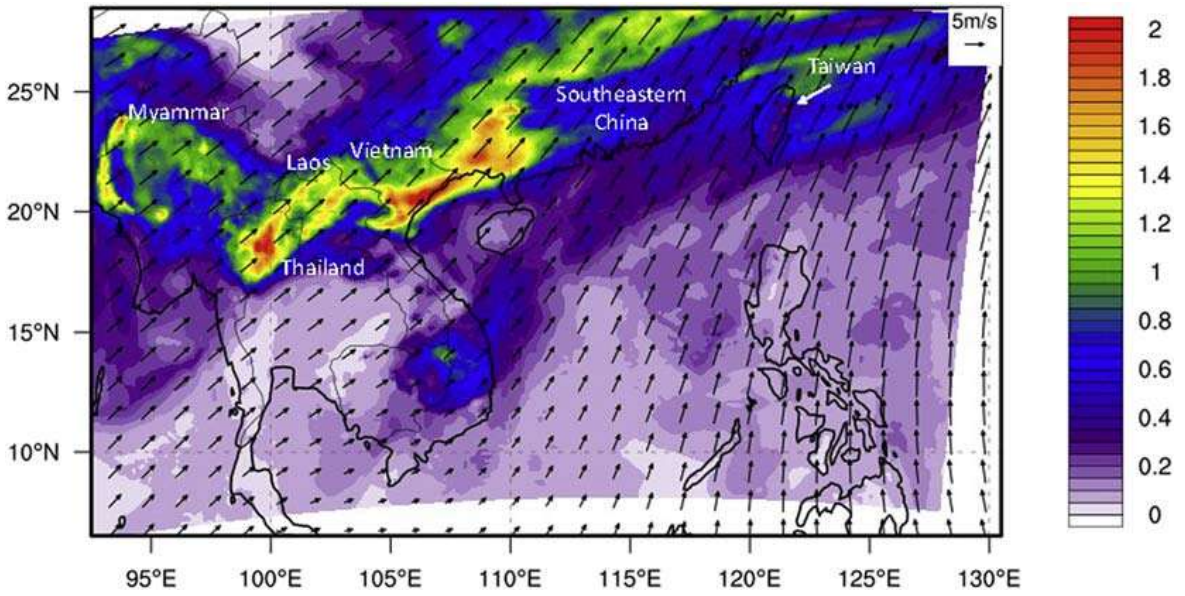

FIGURE 10.7

Modeled Aerosol Optical Depth from WRF-CMAQ output for the biomass burning over Indochina that transported eastwards toward western north Pacific Ocean during the case on March 20, 2013.

Adapted from (Ooi et al., 2021).

plumes into the subtropical westerlies jet and be carried over a larger distance toward the western North Pacific Ocean (Lin et al., 2013). Recently, it was found that the coexistence of the anticyclone over South China Sea is essential for the eastward transport of the emission plume (Huang et al., 2020). The burning pollutant from Indochina is found to be carried to western North Pacific Ocean and was detected at the Taiwan background receptor sites more than 1500 km away as shown in Fig. 10.7 (Chuang et al., 2014). The overhead of biomass burning plume might sink to the surface in circumstances that there are high-pressure system exiting the Asian continent. The physical and chemical properties of the BBA are also subjected to change to the coexistence of Asian dust storm that is frequent during the same season (Dong et al., 2018).

4.3 Case study: Maritime continent

The region experiences tropical wet climate condition according to the Köppen climate classification, while the heterogeneity of land and ocean has complicated the out-of-phase monsoon meteorology over different areas of the region (Ooi et al., 2017). The monsoon meteorology is an important factor of the burning and aerosol transport across the Southern Asian region (Reid et al., 2013). The burning in the MC usually occurs in the summer (June–October) over the Sumatra and Borneo islands, including Indonesia and Malaysia, and produces a large amount of burning emission (Oozeer et al., 2020). The burning is mainly initiated by agricultural activities, while it is sustained under the drier and warmer weather anomalies. The burning over the MC region produces large amounts of burning emission, mainly from the underground peatland fire. The burning in the region is highly susceptible by the dry weather anomaly, especially the eastern pacific ENSO, positive IOD, and dry phase MJO (Amirudin et al., 2020; Latif et al., 2018).

The movement of the haze is subjected to the southwest monsoon above equator and southeast monsoon below equator. In other words, the polluted airmass from the Southern Kalimantan (below equator) moves north-westwards and turns toward northeast direction after crossing the equator into the northern part to the Kalimantan. Similar condition applies for the biomass burning plumes from the Sumatra that travels north-eastwards to the Peninsular Malaysia and eventually entering the South China Sea. There are unusually early haze transport across the Peninsular Malaysia toward northern SEA in the June (e.g., 2013) that occurred due to the presence of tropical cyclones in the South China Sea (Oozeer et al., 2020; Cohen et al., 2017). The low-pressure system has prompted the movement of haze when Typhoon Bebinca has fully developed on 22 June off the coast of Vietnam as seen in Fig. 10.8. The BBA haze has also been found to negatively correlate to the precipitation through AOD and satellite products, reconfirming the role of BBA on climate forcing (Ng et al., 2017).

4.4 Case study: Australia bushfire

Under conducive weather condition, the fire could grow into extreme large fire where the moisture entrained into the burning plume would condense and release large amounts of heat and energy that continue to enhance the deep convection, known as pyroconvection. The clouds formed under such

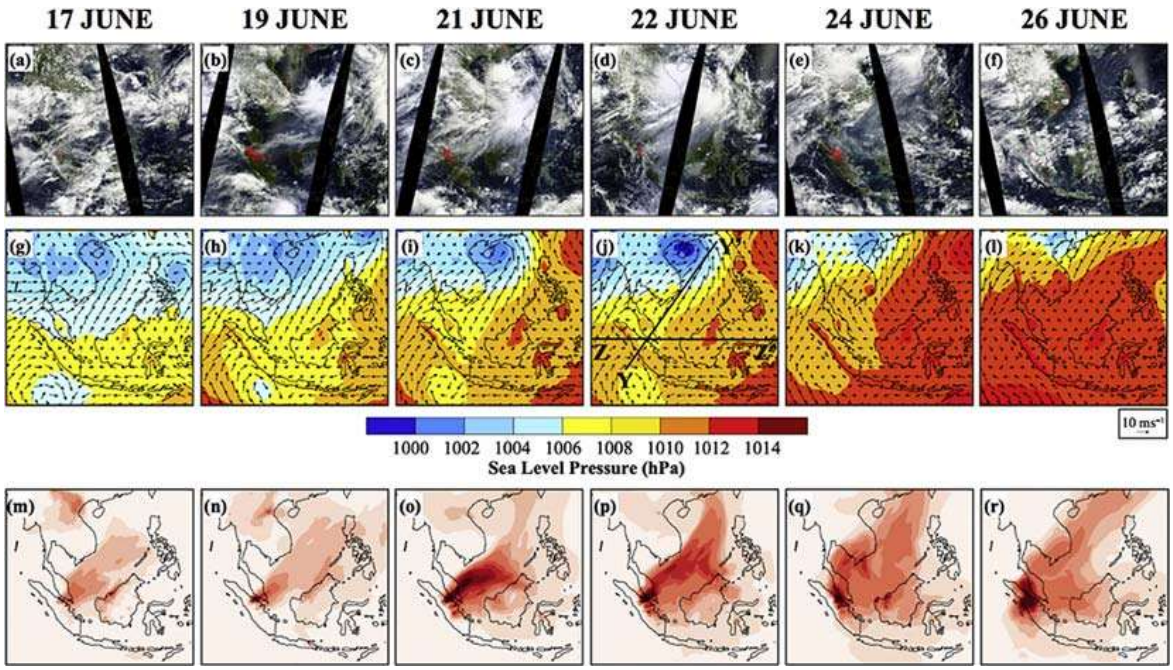

FIGURE 10.8

A case study (June 17, 2013–June 26, 2013) of $PM_{2.5}$ transport in the Maritime Continent from Sumatra toward the Southeast Sea due to the presence of tropical cyclones. First row is the MODIS satellite images, second row is the modeled sea level pressure and surface wind speed from WRF-Chem, third row is the surface $PM_{2.5}$ concentration.

Directly extracted from (Oozeer et al., 2020).

conditions are known as pyrocumulus (PyCu) and pyrocumulonimbus (PyCb) clouds. The deep convection can eventually lead to rainout on one side, while burning intensified on the other side due to the pressure gradient-driven wind gust. The large heat produced such positive feedback of the rainout and continuous release of heat for deep convection, which resembles a weather system itself (Bureau of Meteorology Australia, 2018). Under such an unstable atmospheric condition, the PyCb formed would evolve into thunderstorm and with possibility of lightning as ignition source for burning. The precipitation in the rain has subsequently evaporated due to the dry weather and creates strong downburst, further fueling the upstream burning.

The intense burning produced a large amount of heat that lifts the plume up above surface where the entrained water vapor has condensed to form clouds with the presence of the suspended aerosol as CCN. The thick carbonaceous aerosol particles would absorb solar radiation from reaching the surface and widening the temperature difference between surface and the environment, further enhancing the plume rise. Such situation has occurred during the 2019–20 Australia bushfire, also known as Black Summer. The plume injection height has reached approximately 16 km which can be well considered as lower stratosphere. It is also discovered that the PyCb has changed the stratospheric wind due to the heat absorbed by BBA as well as the stratospheric composition of CO_2, H_2O, O_3, and N_2O (Kablick et al., 2020). Also due to the height attained, the burning haze from the bushfire has been found to have drifted almost 10,000 km across the Pacific Ocean and arrived in Latin America at a height of 6 km (Kablick et al., 2020). Unfortunately, the future climate has found to increase the risk of extreme fire and pyroconvection in the southern Australia, inclusive of the highly populated southeast and southeast Australia (Dowdy et al., 2019).

5. Fire prediction model

Predictability of fire occurrence for emergency response plan requires the evaluation of the potential risk at targeted area and period, where action of prevention and remediation can be taken. This is able to reduce the chances of fire to grow out of hand. The early warning system for wildfire is hence a crucial guide for fire managers to understand the burning condition and plan ahead for the fire suppression effort. The wildfire danger rating tool is widely used to evaluate the fire risk based on the fuel availability, fuel characteristics, and weather condition. The integration of real-time monitoring data and forecasted weather into the existing fire danger rating tool has greatly improved the predictability of the fire risk.

5.1 Historical and continual monitoring

5.1.1 Fire-risk area mapping

Fire-prone area is contributed by several factors, but mainly the availability of the fuel. The mapping of the burning fuel needs to include information about the land cover and soil cover types. Land cover that is easily wilted under the dry weather and soil condition needs to be marked for high risk. Apart from fuel, mapping also involves the extent of destruction severity. Fire-prone areas that are close to human activities, residential, or infrastructure need to be designated with higher risk, for early detection. The risk mapping can finally be revised through the historical burning cases using the postburning scars and burned area product that is characterized by the vegetation cover change, burning ash, and charcoal deposits. Since most of the fires are man-made, tracing back recurring fire cases would be helpful to predict the possibility of next fire onsets.

5.1.2 Detection of fire burning

The common real-time detection of the fire burning is through witness reporting and ground sensors. The latter is rather passive and is usually based on a much larger scale to be seen and hence reported. Located over a fire-prone area, the terrestrial infrared or multimodal sensors mounted on elevated towers detect the immediate on-going fire. Complementing the small-scale coverage of the terrestrial sensor, the surveillance in fire-prone areas should be escalated through timely aerial monitoring and space-borne sensors to detect fire hotspot, burnt area, and fire emission. The real-time and near real-time detection keeps a lookout for thermal anomalies to identify burning hotspots. Technologies used involve small-scale aerial surveillance covered by drone or unmanned aerial vehicle monitoring up to regional and global coverage (Tsay et al., 2016). The Fire Information for Resource Management System (FIRMS) by NASA hosts global active fire data from MODIS sensors aboard NASA's Terra and Aqua satellites and VIIRS aboard Suomi NPP and NOAA-20 satellites. These polar orbiting satellites provide two datasets of global active fire daily, while the geostationary satellites provide continuous monitoring on a regional scale such as European Space Agency's (ESA) MSG-SEVIRI and NASA's GOES-16 ABI. These global sensors also detect fire smoke by retrieving the total column AOD to identify the potential fire emission. On top of the aerosol detection, ESA Copernicus Sentinel-5P's TROPOMI also provides global atmospheric composition for fire relevant emission. The AHI 8/9 sensor aboard Japanese Meteorology Agency's Himawari 8/9 satellite covers the East Asia and Western Pacific regions for aerosol detection efforts.

More specific sensors for analyzing the aerosol properties are available to identify the particle types and amount. The CALIOP sensor aboard the Cloud-Aerosol Lidar and Infrared Pathfinder Satellite Observation (CALIPSO) environmental satellite uses the top-down lidar system to identify the vertical profile of aerosol properties and diagnose the aerosol types including burning aerosols along the global swath. The Multi-angle Imaging SpectroRadiometer (MISR) onboard NASA Terra is able to detect the height of the biomass burning emission via the multiangle camera with different wavelengths. With the vertical dissection of aerosol distribution on different layers, the amount and types of aerosols could be identified diagnostically. More information on the satellite products is provided in Table 10.3.

5.2 Forest fire danger rating system

Fire danger indices have integrated meteorological and fuel availability to serve as warning indicator for potential fire risk over a large area and reference for fire managers on the fire containment effort. Several popularly used fire danger indices are the Canadian Forest Fire Danger Rating System, US National Fire Danger Rating System (NFDRS), and the forthcoming Australian Fire Danger Rating System (AFDRS). There are several components in the fire danger rating system, namely potential weather-associated fire danger and fire behavior rating that evaluate the existing fire behavior. The fire weather rating system that corresponds to the effect of climate change is discussed in this context. The rating system evaluates fire risk according to the weather condition. Weather conditions can influence the fire risk through the near-surface and vertical atmospheric stability.

5.2.1 Fire weather rating system

The near surface maximum temperature, low atmospheric moisture content, and maximum wind speed are critical in conditioning the fuel and soil for burning. There are several popular near-surface fire weather rating systems available, namely Fire Weather Index (FWI) by the Canadian Forest Service

Table 10.3 Available satellite products for near real-time fire burning detection with global and regional coverage.

	Product	Satellites	Source
MODIS active fire product	Active fire hotspot, aerosol detection and properties, and burned area product	NASA Terra/Aqua	https://earthdata.nasa.gov/earth-observation-data/near-real-time/firms/c6-mcd14dl
VIIRS active fire product (VNP14IMGTDL_NRT)	Active fire hotspot	Suomi NPP, NOAA-20	https://earthdata.nasa.gov/earth-observation-data/near-real-time/firms/viirs-i-band-active-fire-data
Advanced Very-High-Resolution Radiometer (AVHRR/3)	Active fire hotspot	NOAA POES, MetOp	https://www.ssd.noaa.gov/PS/FIRE/Layers/FIMMA/fimma.html
Spinning Enhanced Visible and Infrared Imager (SEVIRI)	Active fire hotspot, aerosol detection and properties, and vegetation cover	ESA Meteosat Second Generation (MSG)	https://eumetsat.int/seviri
Advanced Baseline Imager (ABI)	Active fire hotspot, aerosol detection and properties	NASA GOES-16	https://www.goes-r.gov/spacesegment/abi.html
Advanced Himawari Imager (AHI) 8/9	Aerosol optical thickness	JMA Himawari-8/9	https://www.data.jma.go.jp/mscweb/en/product/product_AOT.html
TROPOspheric Monitoring Instrument (TROPOMI)	Aerosol detection and atmospheric composition	ESA Copernicus Sentinel-5P	https//tropomi.eu
Cloud-Aerosol Lidar with Orthogonal Polarization (CALIOP)	Vertical column of aerosol characteristics	NASA CALIPSO	https://www-calipso.larc.nasa.gov/
Multi-angle Imaging SpectroRadiometer (MISR)	Vertical structure of aerosol characteristics	NASA Terra	https://misr.jpl.nasa.gov/
AErosol RObotic NETwork (AERONET)	Bottom-up AOD data	NASA ground network	https://aeronet.gsfc.nasa.gov/
NASA MicroPulse Lidar NETwork (MPLNET)	Bottom-up vertical aerosol characteristics	NASA ground network	https://mplnet.gsfc.nasa.gov/

and McArthur Forest Fire Danger Index (FFDI) by Australia. FWI has provided a general fire risk prediction by encompassing the weather information with three classes of fuel moisture code (Turner and Lawson, 1978). It is one of the most widely adopted fire risk index globally, including Europe, East Asia, and SEA. It includes Fine Fuel Moisture Code (FFMC) to indicate the surface fine fuel that can be easily ignited, Duff Moisture Code (DMC) as fuel made up of organic and woody with average

moisture content, and Drought Code (DC) on the deep layer compact organic matter that is highly subjected for smoldering. The initial fire accounts the influence on wind speed on the surface fuels (FFMC), while the continually buildup of fire is determined by the fuels (DMC and DC) that sustain the burning. The detailed consideration of the fuel moisture code with time-lag difference includes the empirical representation of drought that takes longer time to be sufficiently ready for burning and more tough to contain. Nevertheless, the standard fuel moisture code in FWI is solely based on standard pine as burning fuel which needs to be made if applied to other forest regions.

The NFDRS developed by the US Department of Agriculture has covered additional information on the fuel and fire occurrence risk (Cohen and Deeming, 1985). The system has accounted for the dead and live fuel separately with a distinct moisture content algorithm. The fire ignition source such as human-caused and lightning-caused are also considered in the NFDRS, while the Canadian system has planned but yet to roll out in the Fire Occurrence Prediction system. With the details, the NFDRS is able to model different fire areas with higher accuracy, but the simplicity of FWI garnered greater application without compromising much of its accuracy. The McArthur FFDI used in AFDRS is a more straightforward empirical exponential function that integrates near-surface relative humidity, temperature, and wind speed with drought fraction. The latter is determined through fuel availability under circumstances of soil moisture deficit.

5.2.2 Fire weather stability index

Separate fire weather index is developed to account for the buildup and growth of the extreme or catastrophic fire due to the larger vertical scale atmospheric condition. The Haines Index (HI) developed and used in North America considers the atmospheric stability terms and moisture terms of the lower troposphere using temperature difference and dew point depression, respectively, over two vertical atmospheric layers. The HI is extended to over midtropospheric level to formulate Continuous Haines Index (CHI) as an indicator to determine the vertical stability and dry condition with the near surface condition that is relevant with the pyroconvective processes that often strike the southeast Australia. The CHI is found effective in determining the growth of large fires.

6. Conclusion and way forward

The interactions between wildfire, haze, and climate are interconnected. The influence of climate on biomass burning is clear. The intense heat and less precipitation during the dry season are expected to increase the availability of fuel moisture to burn and for fire to sustain. The weather condition is also decisive on the accumulation, dispersion, as well as the transport of the BBH. On the other hand, the influence of biomass burning and its haze on climate is also clear that the BBA is able to alter the precipitation pattern by inhibiting drizzle and form a larger scale thunderstorm through pyro-convection. From which, the emission from the fire can cause a small-scale weather or even regional displacement of atmospheric composition as well as affecting the stratospheric layer. Nevertheless, the knowledge on the aerosol-radiative cloud feedback processes to the climate still remains to be filled in.

The IPCC has used the RCP to represent radiation forcing of the substance within the atmosphere in the fifth assessment report (AR5), while in the sixth assessment report (AR6), shared socioeconomic pathways are adopted. In other words, the future climate projection is decided upon the socioeconomic activities and plan that governs the source of these radiative forcing. Improvement can be done through

societal decision, so does the deterioration. For an example, the potential change imposed by the climate change in the fire burning is the conversion of land cover, especially on forest. The burning of the rainforest such as in the Amazonian forest would take a longer time to recover or might not even self-replenish, which eventually turn the forest into a shrubland region similar to Africa. This is definitely one of the undesired possibility, but not the only one.

Emergency response during burning cases is hence important, through the accumulation of knowledge and experience from historical cases. Immediate study and data collection on the burnt area, fire spread, fire type, and weather condition need to be documented and analyzed to develop the future remediation plan. A synergic work of ground-based network, remote sensing, and modeling for warning system on this subject shall be considered for the fire prevention, control, and containment effort.

Acknowledgment

This research was funded by the UKM-YSD Chair in Climate Change (code: ZF-2020-001). This work is also partly sponsored by the Shanghai International Science and Technology Cooperation Fund (No. 19230742500).

References

Akagi, S.K., et al., 2011. Emission factors for open and domestic biomass burning for use in atmospheric models. Atmospheric Chemistry and Physics 11 (9), 4039–4072.

Amirudin, A.A., Salimun, E., Tangang, F., Juneng, L., Zuhairi, M., 2020. Differential influences of teleconnections from the Indian and Pacific oceans on rainfall variability in Southeast Asia. Atmosphere (Basel) 11 (9), 13–15.

Andreae, M.O., et al., 2004. Smoking rain clouds over the Amazon. Science (80-) 303 (5662), 1337–1342.

Andreae, M.O., Merlet, P., 2001. Emission of trace gases and aerosols from biomass burning. Global Biogeochemical Cycles 15 (4), 955–966.

BBC News, 31-Jan. Australia Fires: A Visual Guide to the Bushfire Crisis. BBC News, London, England.

Brando, P.M., et al., 2019. Droughts, wildfires, and forest carbon cycling: a pantropical synthesis. Annual Review of Earth and Planetary Sciences 47, 555–581.

Bureau of Meteorology Australia, 2018. When Bushfires Make Their Own Weather. BOM [Online]. Available: https://media.bom.gov.au/social/blog/1618/when-bushfires-make-their-own-weather/. (Accessed 1 July 2021).

CBS News, 27-Aug. Brazil's Bolsonaro Says He Will Accept Aid to Fight Amazon Fires. CBS News, New York, US.

Chang, D.Y., et al., 2021. Direct radiative forcing of biomass burning aerosols from the extensive Australian wildfires in 2019-2020. Environmental Research Letters 16 (4).

Chen, J., et al., 2017a. Science of the Total Environment A review of biomass burning : emissions and impacts on air quality , health and climate in China. Science of the Total Environment 579 (November 2016), 1000–1034.

Chen, J., et al., 2017b. A review of biomass burning: emissions and impacts on air quality, health and climate in China. Science of the Total Environment 579 (November 2016), 1000–1034.

Chuang, M.T., et al., 2014. Carbonaceous aerosols in the air masses transported from Indochina to Taiwan: long-term observation at Mt. Lulin. Atmospheric Environment 89, 507–516.

Cohen, J.E., Deeming, J.D., 1985. The national fire-danger rating system: basic equations. General Technical Reports 16.

Cohen, J.B., Lecoeur, E., Ng, D.H.L., 2017. Decadal-scale relationship between measurements of aerosols, land-use change, and fire over Southeast Asia. Atmospheric Chemistry and Physics 17 (1), 721–743.
Daniel, N.G., Kevin, R.C., Leonard, D.F., 2008. Effects of Fire on Soil and Water. Ogden, UT.
Darmenov, A.S., da Silva, A., 2015. The quick fire emissions dataset (QFED) - documentation of versions 2.1, 2.2 and 2.4. Technical Report Series on Global Modeling and Data Assimilation 38 (September).
Dong, X., Fu, J.S., Huang, K., Lin, N.H., Wang, S.H., Yang, C.E., 2018. Analysis of the Co-existence of long-range transport biomass burning and dust in the subtropical west pacific region. Science Report 8 (1), 1–10.
Dowdy, A.J., et al., 2019. Future changes in extreme weather and pyroconvection risk factors for Australian wildfires. Science Report 9 (1), 1–11.
Giglio, L., Randerson, J.T., Van Der Werf, G.R., 2013. Analysis of daily, monthly, and annual burned area using the fourth-generation global fire emissions database (GFED4). Journal of Geophysical Research: Biogeosciences 118 (1), 317–328.
Gill, P., 06-Jan. Amazon Wildfires Will Cost Brazil Trillions of Dollars— Damage from Australia's Bushfires Maybe 5 Times Greater. Business Insider India, New Delhi, India.
Harris, S., Lucas, C., 2019. Understanding the variability of Australian fire weather between 1973 and 2017. PLoS One 14 (9).
Harris, N., Minnemeyer, S., Stolle, F., Payne, O., 16-Oct. Indonesia's Fire Outbreaks Producing More Daily Emissions than Entire US Economy. World Resrouces Institute, Washington, DC, USA.
Hobbs, P.V., Reid, J.S., Kotchenruther, R.A., Ferek, R.J., Weiss, R., 1997. Direct radiative forcing by smoke from biomass burning. Science (80-) 275 (5307), 1777–1778.
Hoelzemann, J.J., Schultz, M.G., Brasseur, G.P., Granier, C., 2004. Global Wildland Fire Emission Model (GWEM): Evaluating the use of global area burnt satellite data. Journal of Geophysical Research 109 (D14S04), 1–18. https://doi.org/10.1029/2003JD003666.
Hu, Y., Fernandez-Anez, N., Smith, T.E.L., Rein, G., 2018. Review of emissions from smouldering peat fires and their contribution to regional haze episodes. International Journal of Wildland Fire 27 (5), 293–312.
Huang, H.Y., et al., 2020. Influence of synoptic-dynamic meteorology on the long-range transport of Indochina biomass burning aerosols. Journal of Geophysical Research: Atmospheres 125 (3).
Huang, X., Rein, G., 2019. Upward-and-downward spread of smoldering peat fire. Proceedings of the Combustion Institute 37 (3), 4025–4033.
Huang, W.-R., Wang, S.-H., Yen, M.-C., Lin, N.-H., Promchote, P., 2016. Interannual variation of sprintime biomass burning in Indochina: regional differences, associated atmospheric dynamical changes, and downwind impacts. Journal of Geophysical Research: Atmospheres 121, 1–13.
IPCC, 2014. Climate Change 2014: Synthesis Report. Contribution of Working Groups I, II and III to the Fifth Assessment Report of the Intergovernmental Panel on Climate Change. Geneva, Switzerland.
Ito, A., Penner, J.E., 2004. Global Estimates of Biomass Burning Emissions Based on Satellite Imagery for the Year 2000. Journal of Geophysical Research 109 (D14S05), 1–18. https://doi.org/10.1029/2003jd004423.
Jin, Y., et al., 2015. Identification of two distinct fire regimes in Southern California: implications for economic impact and future change. Environmental Research Letters 10 (9).
Kablick, G.P., Allen, D.R., Fromm, M.D., Nedoluha, G.E., 2020. Australian PyroCb smoke generates synoptic-scale stratospheric anticyclones. Geophysical Research Letters 47 (13).
Kaiser, J.W., et al., 2012. Biomass burning emissions estimated with a global fire assimilation system based on observed fire radiative power. Biogeosciences 9 (1), 527–554.
Kang, S., Zhang, Y., Qian, Y., Wang, H., 2020. A review of black carbon in snow and ice and its impact on the cryosphere. Earth-Science Review 210 (August), 103346.
Latif, M.T., et al., 2018. Impact of regional haze towards air quality in Malaysia: a review. Atmospheric Environment 177, 28–44.

Lin, N.-H., et al., Oct. 2013. An overview of regional experiments on biomass burning aerosols and related pollutants in Southeast Asia: from BASE-ASIA and the Dongsha Experiment to 7-SEAS. Atmospheric Environment 78, 1–19.

Liu, T., et al., 2020. Diagnosing spatial biases and uncertainties in global fire emissions inventories: Indonesia as regional case study. Remote Sensor Environment 237 (November 2019), 111557.

McCarty, J.L., Smith, T.E.L., Turetsky, M.R., 2020. Arctic fire re-emerging. Nature Geoscience 13 (10), 658–660.

McKirdy, E., 29-Oct. Southeast Asia' Haze Crisis: A 'crime against Humanity. *CNN*, Atlanta, GA, US.

Michelle, W., et al., 2020. Impact of 2019-2020 mega-fires on Australian fauna habitat. Nature Ecology and Evolution 4, 1321–1326.

Ng, D.H.L., Li, R., Raghavan, S.V., Liong, S.Y., 2017. Investigating the relationship between aerosol optical depth and precipitation over Southeast Asia with relative humidity as an influencing factor. Science Report 7 (1), 1–13.

Ooi, M., et al., 2021. Improving prediction of trans-boundary biomass burning plume dispersion: from northern peninsular Southeast Asia to downwind western north Pacific Ocean. Atmospheric Chemistry and Physics 1–36.

Ooi, M.C.G., Chan, A., Subramaniam, K., Morris, K.I., Oozeer, M.Y., 2017. Interaction of urban heating and local winds during the calm inter-monsoon seasons in the tropics. Journal of Geophysical Research: Atmospheres 122, 1–25.

Oozeer, Y., et al., 2020. The uncharacteristic occurrence of the June 2013 biomass-burning haze event in Southeast Asia: effects of the Madden-Julian oscillation and tropical cyclone activity. Atmosphere (Basel) 11 (55), 1–24.

Pani, S.K., et al., 2021. Brown carbon light absorption over an urban environment in northern peninsular Southeast Asia. Environment Pollution 276, 116735, 2.

Porter, T.W., Crowfoot, W., Newsom, G., 2020. 2019 Wildfire Activity Statistics. California, US.

Quiggin, J., 10-Jan. Australia Is Promising $2 Billion for the Fires. I Estimate Recovery Will Cost $100 Billion. CNN Business, Hong Kong.

Ramanathan, V., Carmichael, G., 2008. Global and regional climate changes due to black carbon. Nature Geoscience 1 (4), 221–227.

Reid, J.S., et al., 2013. Observing and understanding the Southeast Asian aerosol system by remote sensing: an initial review and analysis for the Seven Southeast Asian Studies (7SEAS) program. Atmospheric Research 122, 403–468.

Rosenfeld, D., et al., 2008. Flood or drought: how do aerosols affect precipitation? Science (80-.) 321 (5894), 1309–1313.

Santoso, M.A., Christensen, E.G., Yang, J., Rein, G., 2019. Review of the transition from smouldering to flaming combustion in wildfires. Frontiers of Mechanical Engineering 5 (September).

Simoneit, B.R.T., 2002. Biomass Burning - A Review of Organic Tracers for Smoke from Incomplete Combustion, 17 no. 3.

Tsay, S.C., et al., 2016. Satellite-surface perspectives of air quality and aerosol-cloud effects on the environment: an overview of 7-SEAS/BASELInE. Aerosol and Air Quality Research 16 (11), 2581–2602.

Turetsky, M.R., Benscoter, B., Page, S., Rein, G., Van Der Werf, G.R., Watts, A., 2015. Global vulnerability of peatlands to fire and carbon loss. Nature Geoscience 8 (1), 11–14.

Turner, J.A., Lawson, B.D., 1978. Weather in the Canadian forest fire danger rating system: a user guide to national standards and practices. Rep. BC-X-177 40.

U.S. Department of the Interior, 2018. New Analysis Shows 2018 California Wildfires Emitted as Much Carbon Dioxide as an Entire Year's Worth of Electricity. Press Releases [Online]. Available at: https://www.doi.gov/pressreleases/new-analysis-shows-2018-california-wildfires-emitted-much-carbon-dioxide-entire-years [Accessed: 01-Jul-2021].

Van Der Werf, G.R., et al., 2017. Global fire emissions estimates during 1997-2016. Earth System Science Data 9 (2), 697–720.

Wang, J., et al., 2018. Light absorption of brown carbon in eastern China based on 3-year multi-wavelength aerosol optical property observations and an improved absorption Ångström exponent segregation method. Atmospheric Chemistry and Physics 18 (12), 9061–9074.

Wang, D., et al., 2020. Economic footprint of California wildfires in 2018. Nature Sustainability 4, 252–260.

Werner, J., Lyons, S., 05-Mar. The Size of Australia's Bushfire Crisis Captured in Five Big Numbers. ABC News, New York, US.

Wiedinmyer, C., et al., 2011. The Fire INventory from NCAR (FINN) – a high resolution global model to estimate the emissions from open burning. Geoscientific Model Development 4, 625–641.

Wiedinmyer, C., Quayle, B., Geron, C., Belote, A., McKenzie, D., Zhang, X., O'Neill, S., Wynne, K.K., 2006. Estimating emissions from fires in North America for air quality modeling. Atmospheric Environment 40 (19), 3419–3432. https://doi.org/10.1016/j.atmosenv.2006.02.010.

Witze, A., 2020. Why Arctic fires are bad news for climate change. Nature 585, 336–337.

World Bank Group, 25-Nov. Indonesia's Fire and Haze Crisis. The World Bank, Washington, DC, USA.

Wuebbles, D.J., Fahey, D.W., Hibbard, K.A., Dokken, D.J., Stewart, B.C., Maycock, T.K., 2017. Climate Science Special Report: Fourth National Climate Assessment, vol. I. Washington, DC, USA.

Yen, M.C., et al., 2013. Climate and weather characteristics in association with the active fires in northern Southeast Asia and spring air pollution in Taiwan during 2010 7-SEAS/Dongsha Experiment. Atmospheric Environment 78 (x), 35–50.

Zuckoff, E., 06-Sep. Carbon Dioxide Released by Amazon Fires Could Hasten Climate Change. CAI News, Woods Hole, MA, US.